KSME

Springer

Journal of Mechanical Science and Technology 35 (9) 2021

Original Article
DOI 10.1007/s12206-021-2106-7

Keywords:
· API-X70 steel
· Crack growth analysis
· Hydrogen embrittlement
· XFEM

Correspondence to:
Yoon-Suk Chang
yschang@khu.ac.kr

Citation:
Kim, D.-H., Sim, J. M., Chang, Y.-S., Baek, U. B. (2021). Hydrogen gaseous effects on fracture resistance of API-X70 estimated by XFEM. Journal of Mechanical Science and Technology 35 (9) (2021) 3829~3835.
http://doi.org/10.1007/s12206-021-2106-7

Received December 18th, 2020
Revised April 5th, 2021
Accepted April 16th, 2021

† This paper was presented at APCFS2020, Booyoung Jeju Hotel & Resort, Jeju, Korea, November 3-7, 2020.
Recommended by Guest Editor Byoung-Ho Choi

Hydrogen gaseous effects on fracture resistance of API-X70 estimated by XFEM

Dong-Hyun Kim[1], Jae Min Sim[1], Yoon-Suk Chang[1] and Un Bong Baek[2]

[1]Department of Nuclear Engineering, Kyung Hee University, 1732 Deogyeong-daero, Giheung-gu, Yongin-si 17104, Korea, [2]Division of Industrial Metrology, Korea Research Institute of Standards and Science, 267 Gajeong-ro, Yuseong-gu, Daejeon 34113, Korea

Abstract Hydrogen embrittlement has been recognized as one of major degradation mechanisms causing the decrease of ductility and fracture toughness of several kinds of materials. In accordance with the demand for hydrogen fuels, it becomes more important to ensure safety of relevant facilities like pressure vessels, storage tanks and so on. The objective of this study is to examine fracture resistance of American Petroleum Institute (API)-X70 steel under highly pressurized hydrogen gaseous condition. The extended finite element method (XFEM) was adopted to predict *J-R* curves via a crack growth simulation approach. At first, preliminary analyses for SM490A carbon steel were carried out to demonstrate applicability of the XFEM, of which result was comparable to test data within 14 %. Subsequently, iterative numerical analyses were conducted to calibrate appropriate damage parameters for the API-X70 steel by using notched round bar specimens. Finally, crack growth simulations of 1T-compact tension (CT) specimens were performed adopting the calibrated parameters. J_{IC} values determined from predicted *J-R* curves were compared with 1/2T-CT CTOD test data and relevant constraint effect was discussed.

1. Introduction

Recently, development of infrastructures for efficient transport and storage of hydrogen has been progressed in various fields including the automotive industry as the increased concern on the use of hydrogen fuels [1]. The hydrogen gas is transferred through pipes and stored in tanks at high pressure conditions. Hydrogen embrittlement (HE) may occur in metals, under these high pressure hydrogen environments, and causes degradation of properties such as loss of ductility and fracture toughness. In particular, since the HE in thin pipes of hydrogen charging station led to several accidents, it is required to maintain inherent strength and toughness even though the hydrogen environment.

While lots of experimental and computational efforts have been devoted to preventing failures caused by hydrogen-induced degradation, the elusive phenomenon and mechanism at high pressure condition were not sufficiently identified. Robertson et al. [2] reviewed several mechanisms of HE debated in previous researches and introduced internal pressure mechanism which is also called as high hydrogen pressure bubble or void. According to this mechanism, hydrogen atom which has smaller size than that of metal atoms can penetrate the bigger one and recombine to form hydrogen molecules, which causes deterioration of the mechanical properties of metal. There are two ways to create environments for HE evaluation. One is to experiment under electrochemical conditions considering corrosion and the other is to carry out the test under hydrogen environmental conditions. Li et al. [3] conducted slow strain rate test (SSRT) under the electrochemically pre-charged conditions. They investigated the relationship between degree of degradation and current density. Yamabe et al. [4] performed SSRT for ten types of stainless steels under high pressure internal and external hydrogen gas conditions. The effect of hydrogen gas was examined by comparing relative reduction in area as well as relationship of stress-strain curves. However, SSRT and fracture toughness tests under high

pressure hydrogen environment have constraints and difficulties. The sealing during experiments shall be considered to maintain the purity of the experimental gas inside autoclave and sufficiently eliminated after the experiment. Additionally, ventilation and separated containment are required to prevent leakage of hydrogen gas that can cause explosions.

The simulation of discontinuities using conventional finite element method (FEM) demands on expensive re-meshing process and high element density [5]. Accordingly, while several alternative simulation techniques like virtual crack closure technique, intra-element method and cohesive zone model and so on have been introduced and frequently used to solve problems, lots of uncertainties remained in the field of simulation. Meanwhile, Gurson-Tvergaard-Needleman (GTN) and Rousselier models which are renowned as classical damage models have been improved and still widely used. Abbassi et al. [6] were conducted comparative study to figure out design parameters for tube hydroforming by using GTN model. Florian et al. [7] dedicated strain based evaluation using experimental and numerical analysis results incorporated in Rousselier model. However, both models need to calibrate a lot of analytical parameters so that they are difficult to apply universally. In order to alleviate these limitations, the extended finite element method (XFEM) was developed by Belytschko and Black, which allows element discontinuities by enriching degree of freedom (DOF) [8]. The XFEM does not require focused meshing to match the crack tip to obtain stress intensity factor and can simulate crack initiation and propagation with relatively small efforts. Swati et al. [9] compared the analysis results by using XFEM with experimental data relating to crack initiation and propagation of carbon fiber reinforced polymers.

In this study, a numerical analysis approach using XFEM incorporated in ABAQUS [10] was adopted to estimate hydrogen induced degradation to the material properties. Preliminary analyses were executed to verify the applicability of the approach based on test results from notched round bar (NRB) and 1T-compact tension (CT) specimen which were constructed by steel marine (SM)490A carbon steel in the previous study [11]. Subsequently, the demonstrated approach was expanded for SSRT simulation of American Petroleum Institute (API)-X70 steel to obtain damage parameters and examine the alteration of them due to the highly pressurized hydrogen gas. The parameters determined from NRB specimens were applied to 1T-CT specimens for prediction of fracture resistance (*J-R*) curves under atmospheric (atm.) and hydrogen environments. Finally, the J_{IC} values obtained from analyses and experiments [12] for standard 1T- and smaller 1/2T-CT specimens were compared to investigate constraint effect at the atm. condition.

2. Analysis method

2.1 Key features of XFEM

In the case of the conventional FEM, not only complex meshing at the crack tip but also re-meshing process are essential to execute contour integral and discontinuity evaluation. On the other hand, XFEM does not require to meet conformity of elements near the crack tip. Because the crack position and path are defined by enrichment function of element which has additional DOF [13]. The enrichment function consisted of Heaviside function and crack tip function to simulate discontinuity. The displacement approximation is given by the following Eq. (1) [14]:

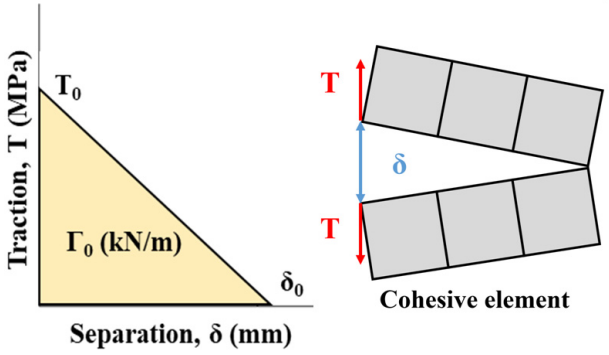

(a) Linear TSL parameters (b) Cohesive element parameters

Fig. 1. Schematics of TSL and cohesive element.

$$u(x)=\sum_{I=1}^{N}N_I(x)[u_I+H(x)a_I+\sum_{\alpha=1}^{4}F_\alpha(x)b_I^\alpha] \quad (1)$$

where the first term denotes usual continuous part consisted of nodal shape function $N_I(x)$ and displacement vector u_I. The term, $H(x)$, is related to discontinuous jump function across the crack surface and nodal enriched DOF I and a. The third term is associated with crack tip consisted of relevant function $F_\alpha(x)$ and nodal enriched DOF b, I and α.

2.2 Analysis procedure

The traction-separation law (TSL) was employed for XFEM, which defines behavior of materials based cohesive segment by the relationship between traction vector (T) and displacement segment vector (δ) as a criterion of propagation. Fig. 1 shows schematics of linear TSL and cohesive element. The parameters of TSL consisted of cohesive strength (T_0), cohesive energy (Γ_0) and critical separation (δ_0). Since the cohesive energy represents the area of Fig. 1(a) as the simplest linear form, T_0 and δ_0 are enough to figure out the relevant parameters for specific materials. The traction and separation of cohesive element at a certain condition are shown in Fig. 1(b).

In particular, maximum principal stress (MAXPS) criterion was selected for damage initiation and evolution governed by the TSL. Damage was initiated when the traction reached the cohesive strength, as the increase of loading, and separation was evolved until critical separation. In order to determine TSL parameters, numerical analyses and comparison with reference data of NRB or SSRT specimens were repeated. Subse-

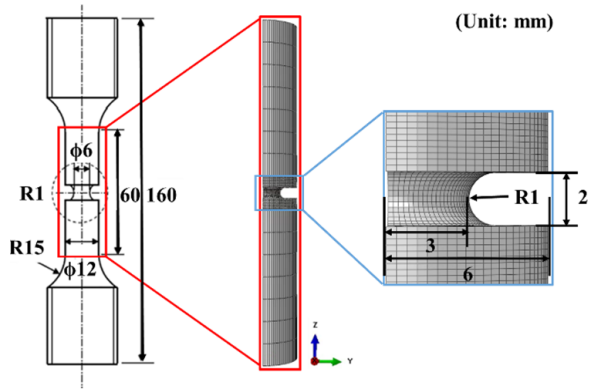

Fig. 2. Schematic and FE model with dimensions for NRB specimen of SM490A carbon steel.

quently, 1T- and 1/2T-CT specimens were analyzed to decide fracture resistance curves using the pre-determined TSL parameters.

3. Verification of analysis process

3.1 Analysis models and conditions

The analysis of NRB specimen made of SM490A carbon steel with 1 mm of notch radius was conducted in order to establish analysis procedure. FE model which is depicted in Fig. 2 was constructed as 1/4 to reduce analysis time taking into account geometrical symmetry. The overall length of the specimen was 60 mm and the diameter of the end section was 12 mm. The height and diameter of notched net section area were set to 2 and 6 mm. Also, the notch radius and depth were modeled as 1 and 3 mm.

The corresponding FE model consisted of 19680 nodes and 17425 elements which is constructed with 3D 8-node element type with a reduced integration (C3D8R). The mechanical properties of the specimen were referred to a previous study [11]. The yz- and xz-planes of the NRB specimen were constrained to the x- and y-directions, respectively. The bottom surface of end section was fully fixed in all directions, and the displacement of 1.5 mm was imposed in the z-direction at opposite surface.

The iterative analyses were conducted to derive TSL parameters. The load (P) versus displacement (δ) curves obtained from experiment and analysis of NRB specimen were shown in Fig. 3. Open and closed symbols represent the analysis and experimental results, respectively. The maximum differences of load and displacement were 0.4 kN and 0.004 mm. The determined TSL parameters were listed in Table 1.

Fig. 4 shows FE model of the half of 3.5 mm pre-cracked 1T-CT specimen which was adopted for crack growth analysis to obtain fracture resistance curve. 10 % of side groove with 45° angle was inserted along each outer surface of specimen. The FE model consisted of 77158 nodes and 72286 C3D8R elements. The element size of crack propagation region was

Table 1. TSL parameters of SM490A carbon steel.

T_0 (MPa)	δ_0 (mm)	Γ_0 (kN/m)
1500	0.200	150

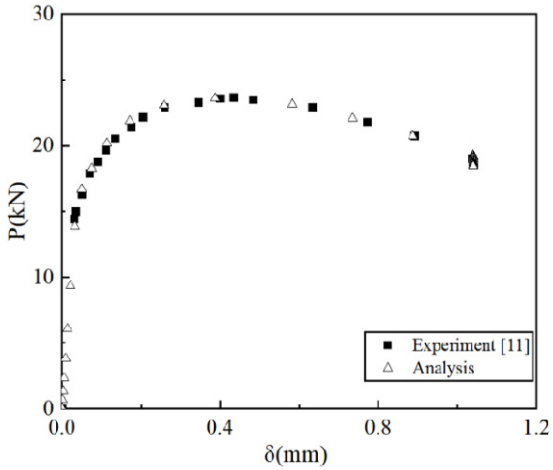

Fig. 3. Comparison of $P-\delta$ curves for NRB specimen of SM490A carbon steel.

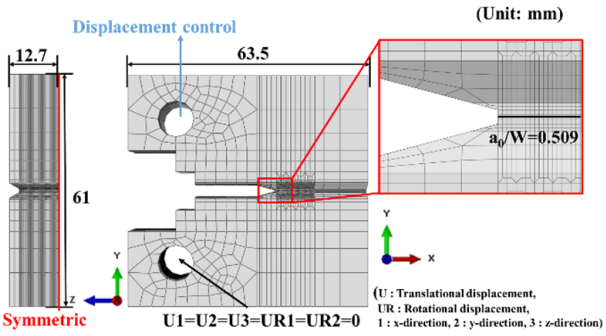

Fig. 4. FE model with dimensions for 1T-CT specimen of SM490A carbon steel.

made as 160 μm considering bias ratio. The TSL parameters determined from the analysis of NRB specimen were applied. As mentioned previously, the specimen was modeled as half in the thickness direction with symmetric condition. Also, loading and boundary conditions were controlled by reference points coupled with neighboring nodes of top and bottom holes. The top hole was moved to y-direction by displacement control and the bottom hole was constrained except for z-axis rotation (UR3).

3.2 Analysis results

Fig. 5 represents the fracture resistance curves of SM490A carbon steel. The open symbol represents analysis result and the closed symbol is experimental data. The decided parameters were applied to crack growth analysis of 1T-CT specimen. J-integral values according to crack extension were calculated following ASTM E1820-13 [15] procedure by using load versus

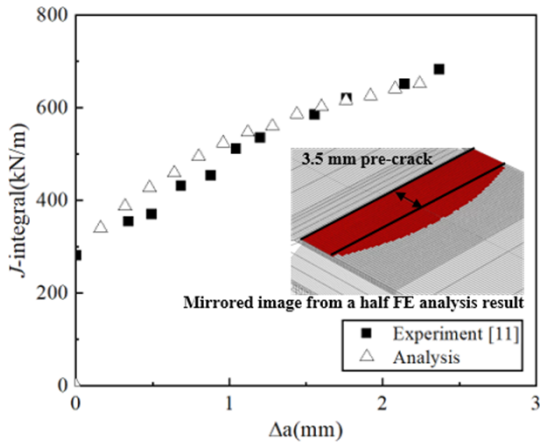

Fig. 5. Comparison of *J-R* curves of SM490A carbon steel.

load-line displacement (LLD) curves. The tendency and values between reference data and analytical one were comparable with the maximum *J*-integral difference of 16.8 kN/m. Also, crack propagation at the center of specimen was faster than outer-most surface one with indicating semi-elliptical shape.

4. Experiments

4.1 Experimental conditions and procedure

API-X70 steel was selected to investigate the effect of hydrogen and its chemical composition is summarized in Table 2. SSRT and fracture toughness tests were conducted under two conditions; one is ambient air with atm. pressure under the room temperature (RT). The other is fulfilled condition by a pressure of 10 MPa in 100 % hydrogen gas under the RT. The NRB specimens were machined as the entire length of 76.2 mm, the end section diameter of 12 mm and the grip section length of 19 mm. Also, notch angle, radius and net section diameter were 60°, 0.083 and 6 mm, respectively. The crack tip opening displacement (CTOD) tests were conducted following the British Standard (BS) 7448-1 [16] using 1/2T-CT specimen due to the limitation of thin thickness of the API-X70 steel pipe. The R = 0.1 fatigue loading ratio and 10 Hz frequency were applied to make pre-crack on 1/2T-CT specimens. The ratio of a_0/W was set to 0.58. The strain rate for NRB specimens was maintained 0.02 mm/s by controlling cross head speed and LLD rate of 1/2T-CT specimens was set to 1 mm/min (0.017 mm/s) as similar.

The pre- and post-treatment processes such as charging, discharging and pressurization were essential in hydrogen environmental experiments. The former process was carried out to maintain the purity of hydrogen gas inside the autoclave and latter process was performed to remove hydrogen gas. Each process was repeated three times, as indicated in ASTM G142 [17]. As a pre-treatment process, the inside of autoclave was made into 99.9 % and 0.5 torr vacuum condition using pump, and the experimental hydrogen gas was compressed to 5 MPa and discharged. After the pre-treatment process, the

Table 2. Chemical composition of API-X70 steel [12].

(wt%)

C	Mn	P	S	Cr	Ni	Cu	Mo	Others
0.07	1.68	0.012	0.01	0.07	0.14	0.1	-	Ni+V+Ti < 0.15

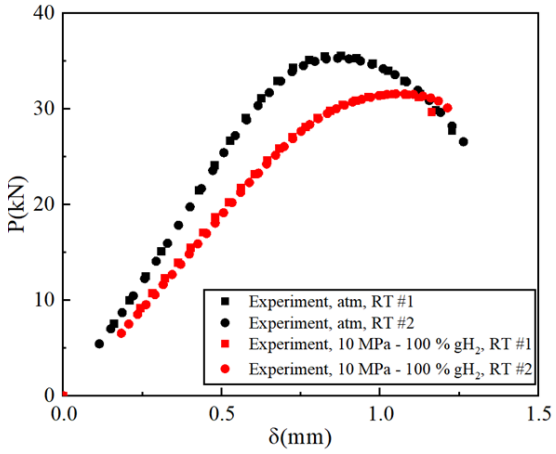

Fig. 6. Comparison of $P-\delta$ curves for NRB specimens of API-X70 steel.

10 MPa of hydrogen gas was filled and maintained for 30 min to check for gas leaks prior to the SSRT and fracture toughness test. After test, the hydrogen gas was eliminated to the initial condition. Nitrogen gas filling and discharging were conducted for autoclave in sequence as a post-treatment process.

4.2 Experimental results

The load-displacement curves measured from experiments for NRB specimen are shown in Fig. 6. The black and red colors represent the atm. and hydrogen conditions, respectively. The ultimate strength and reduction area of NRB specimen were estimated following ASTM G129 [18]. The ultimate strength was reduced from 1251 MPa to 1217 MPa under hydrogen condition. The reduction rate of cross-sectional area was 45.4 % under atm. condition and 21.2 % under hydrogen condition. Measured CTOD values were 0.414 and 0.125 mm for each condition. The CTOD data were converted into *J*-integrals following ASTM E1820-13 [15]. The J_{IC} values were 446.96 and 134.05 kN/m under the atm. and hydrogen conditions, respectively.

5. Assessment of hydrogen gas effects

5.1 Analysis models and conditions

The approach established in the previous section was expanded to predict and evaluate the fracture resistance curves of API-X70 steel under the two kinds of environment for SSRT. Mechanical properties of API-X70 steel dependent on test conditions are summarized in Table 3. Elastic-plastic analyses were carried out under the assumption of isotropic material behavior.

Table 3. Mechanical properties of API-X70 steel.

Test condition	Elastic modulus (GPa)	Poisson's ratio	Yield strength (MPa)	Tensile strength (MPa)
atm., RT	204.9	0.3	601.1	630.9
10 MPa - 100 % gH_2, RT	198.5	0.3	608.7	626.7

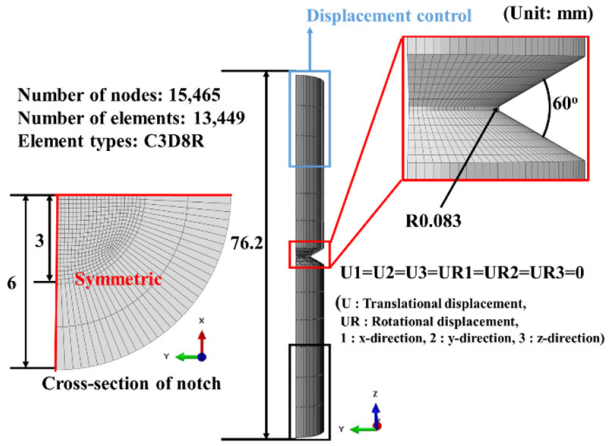

Fig. 7. FE model of NRB specimen of API-X70 steel.

Fig. 7 shows quarter FE models of NRB specimen, which was constructed to reduce analysis time in consideration of geometrical symmetry. It consists of 15465 nodes and 13449 C3D8R elements whether hydrogen gas is charged or not. The size of elements at the center of specimen where fracture will be observed was 150 μm for SSRT simulations. The yz- and xz-planes were fixed to each normal direction using symmetric option. More than two-thirds of the grip section was fully fixed and the displacement of 3 mm in z-direction was applied as a loading condition at the opposite region.

The load-displacement curves of analysis under the two kinds of test conditions were compared with those of experiments plotted in the previous figure. Discrepancies of the maximum displacements between experimental data [12] and analysis results were decided as 0.001 mm. TSL parameters obtained from sufficient calibration and comparable with the experimental results are listed in Table 4. The determined parameters in hydrogen gaseous condition were lower than those of atm. condition. While it seems to be related to hydrogen-induced degradation of aging mechanism details are not covered in this study.

J_{IC} values and fracture resistance curves were predicted for 1T-CT specimen using the TSL parameters. Analysis conditions including model information are the same with those in Fig. 4. Moreover, the crack growth analysis using 1/2T-CT specimen was conducted under atm. condition to investigate different sizes induced constraint effect through comparison with the result of 1T-CT specimen. As in the experiment, the a_0/W ratio was set to 0.58. The 1/2T-CT specimen without side grooves was modeled with 71,012 nodes and 66920 C3D8R

Table 4. TSL parameters of API-X70 steel.

Test condition	T_0 (MPa)	δ_0 (mm)	Γ_0 (kN/m)
atm., RT	1610	0.186	150
10 MPa - 100 % gH_2, RT	1150	0.130	75

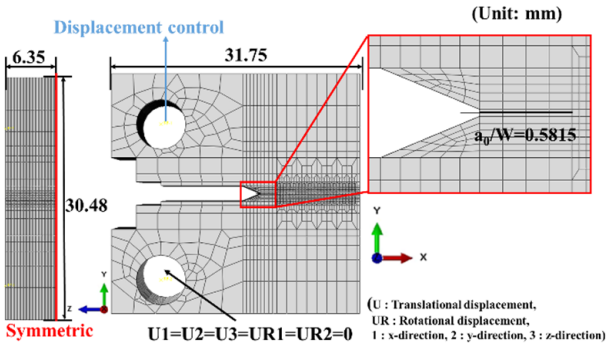

Fig. 8. FE model of 1/2T-CT specimen of API-X70 steel.

elements. Fig. 8 shows the half of FE model with symmetric option. Loading and boundary conditions were also controlled by reference points as in the preliminary analysis of SM490A carbon steel.

5.2 Analysis results and discussion

With regard to the NRB, fracture occurs from the edge of specimen due to stress concentrations at notch when tensile load is applied. The damage was developed and led to fracture when the MAXPS criterion was satisfied.

Fig. 9 delineates not only von Mises contour plots of specimen and enlarged near the crack tip but also crack propagation shape under the hydrogen conditions. The pre-crack under the hydrogen condition grew about 0.68 mm longer than that under the atm. condition, when the LLD was applied as 1.5 mm to the specimens. Crack propagation amounts of the specimens were normalized by the initial ligament of specimen to quantify influence of the hydrogen condition. For example, comparing to the normalized value of 0.01 under the atm. condition, the one under the hydrogen condition was 0.037 at the same LLD condition. It means that the crack became 2.7 times long approximately. Similar to the preliminary analysis, crack propagation at the inner-most surface of specimens was also faster than in the region near the outer-most surfaces due to triaxial stress states. Also, the size of curvature cracks was decided base on ASTM E1820-13 procedure [15].

For 1T-CT specimen, the fracture resistance curves of API-X70 steel were estimated under whether hydrogen gas is charged or not and presented in Fig. 10. The construction lines such as 0.15, 0.2 and 1.5 exclusion lines were also drawn as a function of flow strengths. The coefficients of power law curve fit ($J = C_1(\Delta a)^{C_2}$) were determined by the least square method with linear regression using the data between 0.5 and 1.5 mm exclusion lines. As a result, values of C_1 and C_2 were determined as 800 kN/m and 0.2 under the atm. condition while

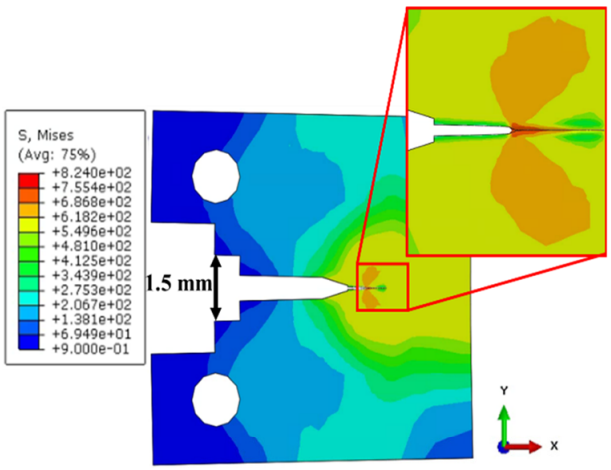

(a) 1/2-model von-Mises distribution

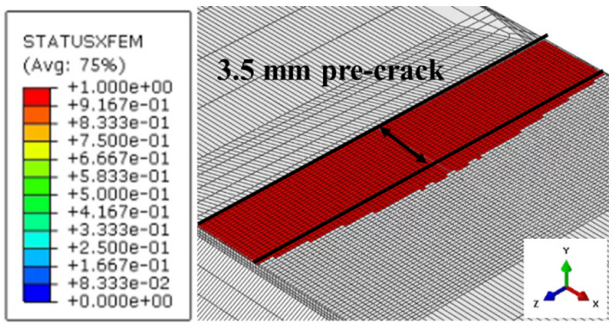

(b) Crack propagation shape mirrored from a half model

Fig. 9. 1T-CT specimen analysis results under 10 MPa - 100 % gH_2, RT condition.

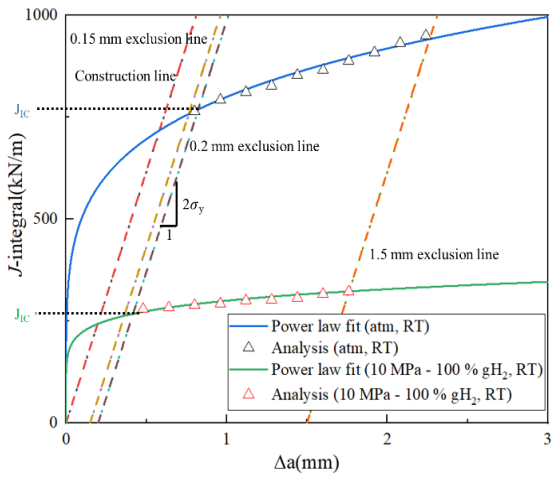

Fig. 10. Predicted *J-R* curves with construction lines dependent on test conditions.

300 kN/m and 0.13 for the exposed one to hydrogen condition. Furthermore, since the provisional J_Q values as intersection points between the fitted power law curve and 0.2 mm exclusion line met the requirements for qualification, they were recognized as valid J_{IC} values. Predicted values of J_{IC} were 768.7 kN/m under the atm. condition and 268.1 kN/m under the hydrogen condition. The differences of J_{IC} with experiments were 321.74 kN/m and 117.3 kN/m for each condition.

Moreover, J_{IC} obtained from an additional crack growth analysis of 1/2T-CT specimen was 459.97 kN/m under the atm. condition, and its difference with experimental result was reasonably 13 kN/m. Similar observation was reported in a couple of previous researches. *J*-integrals determined from smaller specimens were lower than those of the standard specimens in general, which was explained by the constraint effect [19, 20].

6. Conclusions

In this study, a series of XFEM analyses were carried out for NRB, 1T- and 1/2T-CT specimens. Contribution of the hydrogen was evaluated and the conclusions were derived as follows.

1) Numerical analysis procedure was demonstrated by using SM490A carbon steel and compared with its test data from previous study. The maximum difference of predicted and experimental fracture resistance curves was less than 14 %.

2) The validated procedure was expanded to API-X70 steel and its TSL parameters were optimized by NRB specimens under air and hydrogen gaseous environments. The cohesive strength, critical separation and cohesive energy decreased 29, 30 and 50 % under the 10 MPa - 100 % gH_2, RT condition, respectively.

3) Optimized parameters from NRB specimen were applied to 1T-CT specimen, and the crack propagation amount under the hydrogen condition was raised as 270 % at the same LLD. In addition, based on the predicted fracture resistance curves J_{IC} under the hydrogen condition was reduced as 65 % comparing to the air conditional one.

4) Difference of fracture resistance curves occurred between 1T-CT analyses and 1/2T-CT experiments. The reason was addressed by an additional 1/2T-CT analysis as the constraint effect.

Acknowledgments

This work is supported by the Korea Agency for Infrastructure Technology Advancement (KAIA) grant funded by the Ministry of Land, Infrastructure and Transport (Grant 19TLRP-C152334-01).

Nomenclature

$N_I(x)$	: Nodal shape function
u_I	: Displacement vector
$H(x)$	: Heaviside function
$F_\alpha(x)$	: Crack tip function
I, a, b, α	: Nodal enriched degree of freedom
T	: Traction vector
δ	: Displacement segment vector
T_0	: Cohesive strength
δ_0	: Critical separation

Γ_0 : Cohesive energy

References

[1] I. Moro, L. Briottet, P. Lemoine, E. Andrieu, C. Blanc and G. Odemer, Hydrogen embrittlement susceptibility of a high strength steel X80, *Materials Science and Engineering*, A (527) (2010) 7252-7260.

[2] I. M. Robertson, P. Sofronis, A. Nagao, M. L. Martin, S. Wang, D. W. Gross and K. E. Nygren, Hydrogen embrittlement understood, *Metallurgical and Materials Transactions B*, 46B (2015) 1085-1103.

[3] X. Li, J. Zhang, E. Akiyama, Q. Fu and Q. Li, Hydrogen embrittlement behavior of Inconel 718 alloy at room temperature, *Journal of Mechanical Science and Technology*, 35 (4) (2019) 499-502.

[4] J. Yamabe, O. Takakuwa, H. Matsunaga, H. Itoga and S. Matsuoka, Hydrogen diffusivity and tensile-ductility loss of solution-treated austenitic stainless steels with external and internal hydrogen, *International Journal of Hydrogen Energy*, 42 (2017) 13289-13299.

[5] K. H. Schwalbe, I. Scheider and A. Cornec, *Guidelines for Applying Cohesive Models to the Damage Behaviour of Engineering Materials and Structures*, Springer, New York (2013).

[6] F. Abbassi, F. Ahmad, S. Gulzar, T. Belhadj, A. Karrech and H. S. Choi, Design of T-shaped tube hydroforming using finite element and artificial neural networking modeling, *Journal of Mechanical Science and Technology*, 34 (3) (2020) 1129-1138.

[7] F. Florian and S. Michael, Experimental and numerical investigations on limit strains using an enhanced rousselier model, *Engineering Fracture Mechanics*, 226 (2020) 106868.

[8] T. Belytschko and T. Black, Elastic crack growth in finite element with minimal remeshing, *International Journal for Numerical Methods in Engineering*, 45 (5) (1999) 601-620.

[9] R. F. Swati, L. H. Wen, H. Elahi, A. A. Khan and S. Shad, Experimental and numerical investigation of transversal damage in carbon fiber reinforced composites using X-FEM analysis, *Journal of Mechanical Science and Technology*, 33 (1) (2019) 205-211.

[10] ABAQUS, *ABAQUS User's Manual Ver. 2020*, Dassault Systemes, Vélizy-Villacoublay, France (2020).

[11] G. G. Youn, J. S. Kim, Y. J. Kim and M. Kamaya, Numerical prediction of notch bluntness effect on fracture resistance of SM490A carbon steel, *Fatigue & Fracture of Engineering Materials & Structures*, 43 (4) (2020) 660-671.

[12] T. T. Nguyen, J. Park, W. S. Kim, S. H. Nahm and U. B. Beak, Effect of low partial hydrogen in a mixture with methane on the mechanical properties of X70 pipeline steel, *International Journal of Hydrogen Energy,* 45 (2020) 2368-2381.

[13] A. R. Khoei, *Extended Finite Element Method: Theory and Applications*, Wiley (2015).

[14] G. Sivakumar and V. B. Maji, Simulation of crack propagation in rocks by XFEM, *Proc. of the Conference on Recent Advances in Rock Engineering (RARE 2016)*, Atlantis Press (2016).

[15] ASTM E1820-13, *Standard Test Method for Measurement of Fracture Toughness*, ASTM International, West Conshohocken, PA (2013).

[16] ASTM G142-98, *Standard Test Method for Determination of Susceptibility of Metals to Embrittlement in Hydrogen Containing Environments at High Pressure, High Temperature, or Both*, ASTM International, West Conshohocken, PA (2011).

[17] BS 7448-1:1991, *Fracture Mechanics Toughness Tests - Part 1. Method for Determination of KIC, Critical CTOD and Critical J values of Metallic Materials*, British Standard Institution, London, UK (1991).

[18] ASTM G129-00, *Standard Practice for Slow Strain Rate Testing to Evaluate the Susceptibility of Metallic Materials to Environmentally Assisted Cracking*, ASTM International, West Conshohocken, PA (2006).

[19] Y. S. Chang, J. M. Kim, J. B. Choi, Y. J. Kim, M. C. Kim and B. S. Lee, Derivation of ductile fracture resistance by use of small punch specimens, *Engineering Fracture Mechanics*, 75 (2008) 3413-3427.

[20] C. S. Seok and S. Y. Kim, Effect of specimen configurations on the fracture resistance curve, *Nuclear Engineering and Design*, 214 (2002) 47-56.

Dong-Hyun Kim received his B.S. degree from the Department of Nuclear Engineering in 2020 at Kyung Hee University. Currently he is a M.S. candidate in Kyung Hee University and his research interest is computational fracture mechanics.